Highly-Efficient Aerodynamic Optimal Design of Rotor Airfoil Using Viscous Adjoint Method

Wu Qi, *Zhao Qijun* *, *Wang Qing*

National Key Laboratory of Science and Technology on Rotorcraft Aeromechanics, Nanjing University of Aeronautics and Astronautics, Nanjing 210016, P. R. China

(Received 26 May 2015; revised 18 January 2016; accepted 10 February 2016)

Abstract: In order to overcome the efficiency problem of the conventional gradient-based optimal design method, a highly-efficient viscous adjoint-based RANS equations method is applied to the aerodynamic optimal design of hovering rotor airfoil. The C-shaped body-fitted mesh is firstly automatically generated around the airfoil by solving the Poisson equations, and the Navier-Stokes (N-S) equations combined with Spalart-Allmaras (S-A) one-equation turbulence model are used as the governing equations to acquire the reliable flowfield variables. Then, according to multi-constrained characteristics of the optimization of high lift/drag ratio for hovering rotor airfoil, its corresponding adjoint equations, boundary conditions and gradient expressions are newly derived. On these bases, two representative rotor airfoils, NACA0012 airfoil and SC1095 airfoil, are selected as numerical examples to optimize their synthesized aerodynamic characteristics about lift/drag ratio in hover, and better aerodynamic performance of optimal airfoils are obtained compared with the baseline. Furthermore, the new designed rotor with the optimized rotor airfoil has better hover aerodynamic characteristics compared with the baseline rotor. In contrast to the baseline airfoils optimized by the finite difference method, it is demonstrated that the adjoint optimal algorithm itself is practical and highly-efficient for the aerodynamic optimization of hover rotor airfoil.

Key words: rotor airfoil; viscous adjoint method; aerodynamic characteristics; multi-constraints; computational fluid dynamics (CFD); highly efficiency

CLC number: V211.52 **Document code**: A **Article ID**: 1005-1120(2017)02-0134-09

0 Introduction

To design an advanced rotor airfoil shape, it is imperative to consider the special working environment of rotor. For the helicopter, hover state is an important and characteristic state, and it calls for excellent synthesized aerodynamic characteristics for the rotor airfoil[1]. However, even if significant progress has been made in the algorithms and computer hardware during the past decades, an efficient accompanied with multi-constrained design method still seems challenging for designing of the rotor airfoil. Therefore, seeking an efficient aerodynamic design method for the rotor airfoil has aroused great concern in the field of helicopter aerodynamics[2].

There are mainly two types of methods for rotor airfoil shape designing, one is inverse design method and the other is optimization method. For the inverse design method[3,4], it is generally needed to give a target pressure distribution for the rotor airfoil before designing, thus it calls for rich designing experience for designers. What's more, it can seem to be more struggling in dealing with multi-constrained problems. For the optimization method, the airfoil shape is usually parameterized with a set of design variables, and a suitable objective function is chosen to be minimized or maximized. Then through continuous modifications of the baseline airfoil which satisfies some certain geometric and aerodynamic constrains at the same time, the objective function can obtain the ex-

* Corresponding author, E-mail address: zhaoqijun@nuaa.edu.cn.

How to cite this article: Wu Qi, Zhao Qijun, Wang Qing. Highly-efficient aerodynamic optimal design of rotor airfoil using viscous adjoint method[J]. Trans. Nanjing Univ. Aero. Astro., 2017,34(2):134-142.
http://dx.doi.org/10.16356/j.1005-1120.2017.02.134

treme value. For aerodynamic shape optimization, compared with the global optimal technique, e. q. genetic algorithm[5,6], the gradient-based optimal technique is more computational cost saving and widely used. For the later one, finding a fast and accurate way of evaluating the gradient information is the vital part because this occupies a considerable amount of time in the design algorithm. Gradient information can be calculated using a variety of approaches such as the finite-difference method[7], automatic differentiation[8], and complex step method[9]. Whereas for these methods, the amount of computation cost during each step is proportional to number of designing variable, which can restrict their usage in the complex aerodynamic shape optimization to some extent. As an alternative method, the control theory approach has noticeable computational cost advantages over the former. When employing this method, the relevant gradients are obtained through the solution of adjoint equations of the governing equations. Accordingly, the mere cost involved is one flow solution and one adjoint solution during each step, leading to high efficiency of the method despite of number of designing variables.

The continuous viscous adjoint method was firstly used in inviscid transonic flow by Jameson[10-12] in the late 1980s. Since then, the method has achieved a significant breakthrough, and now it can be even used for the aerodynamic design of whole aircraft configurations in viscous flow[13,14]. Specially for the rotor, Lee and Khown[15] have adopted a continuous adjoint method for Euler rotor flows in hover using unstructured mesh. After that, Huang and Yang[16] have conducted a viscous continuous adjoint-based optimization of drag coefficient of rotor airfoil. From these earlier works, it demonstrates the potential capability of the method for the rotor airfoil design. However, Lee et al. doesn't consider the effect of the viscous effect in their research, while optimization design of rotor airfoil of Huang et al. doesn't have a strong relationship with the three-dimensional rotor design. In addition, these studies are also relevant with the problem of single objective, and they still lack the ability of handling the multi-constrained problems for rotor airfoil.

In the present work, an efficient continuous viscous adjoint method, which is extended to handle with the multi-constrained problem, is applied to optimize the aerodynamic shape of rotor airfoil. To better capture the information of the boundary layer, the Spalart-Allmaras (S-A) turbulence model[17] are chosen to close the Navier-Stokes equations. With the aim of higher lift/drag ratio, the corresponding adjoint equations, boundary condition and gradient expression are continually derived. Two representative rotor airfoils, NACA0012 airfoil and SC1095 airfoil, are selected as baseline airfoils to optimize their synthesized aerodynamic characteristics to validate the effectiveness of method. Furthermore, the optimized rotor airfoil is also applied to form three-dimensional rotor to verify its hover aerodynamic characteristics compared with the baseline rotor.

1 Flow Analysis

1.1 Governing equations

The two-dimensional RANS equations are formulated in a calculating coordinate (ξ_1, ξ_2). It can be written as

$$\frac{\partial (J\boldsymbol{w})}{\partial t} + \frac{\partial \boldsymbol{S}_{ij}\boldsymbol{f}_j}{\partial \xi_i} = \frac{\partial \boldsymbol{S}_{ij}\boldsymbol{f}_{vj}}{\partial \xi_i} \tag{1}$$

where $\boldsymbol{w}$ is the vector of conservative variables, $\boldsymbol{f}_j$ the vector of convective fluxes, and $\boldsymbol{f}_{vj}$ is the vector of viscous fluxes. In addition, $\boldsymbol{S}_{ij}$ is the transformation matrix from Cartesian to calculating coordinate, it can be calculated as

$$\boldsymbol{S}_{ij} = J \frac{\partial \xi_i}{\partial \boldsymbol{x}_j} \tag{2}$$

1.2 Numerical resolution of RANS equations

In the current paper, the governing equations are discretized using a finite volume method with cell-centered evaluation of conservative variables. The JST scheme[18] and centered formula are used for the spatial discretisation of the convective fluxes $\boldsymbol{f}_j$ and viscous fluxes $\boldsymbol{f}_{vj}$, and the turbulent

viscosity is calculated with Spalart-Allmaras turbulence model[17]. For temporal discretisation, it is conducted by five-step Runge-Kutta algorithm[18]. To accelerate convergence, the local time step and implicit residual smoothing scheme are also added in the program. The no-slip boundary condition is employed on the wall, and specific for the adiabatic wall, the normal derivative $\partial T/\partial n$ is equal to zero. The non-reflecting condition is used for the far field boundary.

2 Adjoint Method

2.1 Principle of adjoint method

For the aerodynamic shape optimization of rotor airfoil, the objective function can be defined as I, which can be determined by conservative variables of flowfield and airfoil shape

$$I=\int_B \boldsymbol{M}(\boldsymbol{w}(\alpha),\boldsymbol{S}(\alpha))\mathrm{d}B_\xi+\int_D \boldsymbol{P}(\boldsymbol{w}(\alpha),\boldsymbol{S}(\alpha))\mathrm{d}D_\xi \tag{3}$$

where α is the coefficient of the shape function when the Hicks-Henne shape function method[7] is employed to describe the shape of the airfoil in this paper.

For the RANS equations, its steady form can be expressed as

$$\frac{\partial}{\partial \xi_i}(\boldsymbol{F}_i-\boldsymbol{F}_{vi})=0$$
$$\boldsymbol{F}_i=\boldsymbol{S}_{ij}\boldsymbol{f}_j,\boldsymbol{F}_{vi}=\boldsymbol{S}_{ij}\boldsymbol{f}_{vj} \tag{4}$$

Take variation for objective function and steady RANS equations, respectively. Then bring the steady RANS equations as an equality constraints into objective function through this Lagrange multiplier $\boldsymbol{\Psi}=(\Psi_1,\Psi_2,\Psi_3,\Psi_4)^{\mathrm{T}}$. Finally, the variation of objective function, after further transformation, after further transformation, can be expressed as

$$\delta I=\int_B[\delta\boldsymbol{M}-n_i\boldsymbol{\Psi}^{\mathrm{T}}\delta(\boldsymbol{F}_i-\boldsymbol{F}_{vi})]\mathrm{d}B_\xi+\int_D\left[\delta\boldsymbol{P}+\frac{\partial\boldsymbol{\Psi}^{\mathrm{T}}}{\partial\xi_i}\delta(\boldsymbol{F}_i-\boldsymbol{F}_{vi})\right]\mathrm{d}D_\xi \tag{5}$$

Choosing $\boldsymbol{\Psi}$ to meet the adjoint equation (Eq. (6)) and adjoint boundary (Eq. (7))

$$\frac{\partial\boldsymbol{P}}{\partial\boldsymbol{w}}+\frac{\partial\boldsymbol{\Psi}^{\mathrm{T}}}{\partial\xi_i}\left(\frac{\partial\boldsymbol{F}_i}{\partial\boldsymbol{w}}-\frac{\partial\boldsymbol{F}_{vi}}{\partial\boldsymbol{w}}\right)=0 \tag{6}$$

$$\frac{\partial\boldsymbol{M}}{\partial\boldsymbol{w}}-\boldsymbol{n}_i\boldsymbol{\Psi}^{\mathrm{T}}\left(\frac{\partial\boldsymbol{F}_i}{\partial\boldsymbol{w}}-\frac{\partial\boldsymbol{F}_{vi}}{\partial\boldsymbol{w}}\right)=0 \tag{7}$$

Therefore, the variation of objective function can be simplified as

$$\delta I=\left\{\int_B\left[\frac{\partial\boldsymbol{M}}{\partial\boldsymbol{S}}-\boldsymbol{n}_i\boldsymbol{\Psi}^{\mathrm{T}}\left(\frac{\partial\boldsymbol{F}_i}{\partial\boldsymbol{S}}-\frac{\partial\boldsymbol{F}_{vi}}{\partial\boldsymbol{S}}\right)\right]\mathrm{d}B_\xi+\int_D\left[\frac{\partial\boldsymbol{P}}{\partial\boldsymbol{w}}+\frac{\partial\boldsymbol{\Psi}^{\mathrm{T}}}{\partial\boldsymbol{\xi}_i}\left(\frac{\partial\boldsymbol{F}_i}{\partial\boldsymbol{S}}-\frac{\partial\boldsymbol{F}_{vi}}{\partial\boldsymbol{S}}\right)\right]\mathrm{d}D_\xi\right\}\delta\boldsymbol{S} \tag{8}$$

From Eq. (8), it is demonstrated that the gradient solving is now associated with the airfoil shape rather than flowfield variables. Therefore, during the single optimization procedure, the program does not need to call for computational fluid dynamics (CFD) solver repeatedly only at the cost of solving the new introduced adjoint equations. When the number of design variables becomes larger, it can greatly reduce the computation time.

2.2 Adjoint equations and boundary condition

Specified for the two-dimensional RANS equations, after considering the effect of convective fluxes and viscous fluxes on the adjoint equations and boundary condition, the new continuous viscous adjoint equations can be formulated as

$$\boldsymbol{JA}_1^{\mathrm{T}}\frac{\partial\boldsymbol{\Psi}}{\partial x}+\boldsymbol{JA}_2^{\mathrm{T}}\frac{\partial\boldsymbol{\Psi}}{\partial\boldsymbol{y}}+[\boldsymbol{M}^{-1}]^{\mathrm{T}}\boldsymbol{Y}=0$$

$$\boldsymbol{A}_1^{\mathrm{T}}=\begin{bmatrix}0 & -u^2+\frac{\gamma-1}{2}q^2 & -uv & u[-\gamma E+(\gamma-1)q^2]\\ 1 & -(\gamma-3)u & v & \gamma E-(\gamma-1)\left(u^2+\frac{q^2}{2}\right)\\ 0 & -(\gamma-1)v & u & -(\gamma-1)uv\\ 0 & \gamma-1 & 0 & \gamma u\end{bmatrix}$$

$$\boldsymbol{A}_2^{\mathrm{T}}=\begin{bmatrix}0 & -uv & -v^2+\frac{\gamma-1}{2}q^2 & v[-\gamma E+(\gamma-1)q^2]\\ 0 & v & -(\gamma-1)u & -(\gamma-1)uv\\ 1 & u & -(\gamma-3)v & \gamma E-(\gamma-1)\left(v^2+\frac{q^2}{2}\right)\\ 0 & 0 & \gamma-1 & \gamma v\end{bmatrix}$$

$$\boldsymbol{Y}=J\begin{bmatrix}\frac{-a^2\mu}{(\gamma-1)\mathrm{Pr}\rho}\left(\frac{\partial^2\Psi_4}{\partial x^2}+\frac{\partial^2\Psi_4}{\partial y^2}\right)\\ \frac{\partial T_{xx}}{\partial x}+\frac{\partial T_{xy}}{\partial y}+\frac{\partial\tau_{xx}}{\partial x}+\frac{\partial\tau_{xy}}{\partial x}-\sigma_{xx}\frac{\partial\Psi_4}{\partial x}-\\ \sigma_{xy}\frac{\partial\Psi_4}{\partial y}\frac{\partial T_{yx}}{\partial x}+\frac{\partial T_{yy}}{\partial y}+\frac{\partial\tau_{yx}}{\partial x}+\frac{\partial\tau_{yy}}{\partial x}-\sigma_{yx}\frac{\partial\Psi_4}{\partial x}-\\ \sigma_{yy}\frac{\partial\Psi_4}{\partial y}\frac{a^2\mu}{(\gamma-1)\mathrm{Pr}\rho}\left(\frac{\partial^2\Psi_4}{\partial x^2}+\frac{\partial^2\Psi_4}{\partial y^2}\right)\end{bmatrix}$$

$$[\boldsymbol{M}^{-1}]^{\mathrm{T}}=\begin{bmatrix}1 & -\frac{u}{\rho} & -\frac{v}{\rho} & \frac{(\gamma-1)}{2}q^2\\ 0 & \frac{1}{\rho} & 0 & -(\gamma-1)u\\ 0 & 0 & \frac{1}{\rho} & -(\gamma-1)v\\ 0 & 0 & 0 & \gamma-1\end{bmatrix} \tag{9}$$

As for different objective function and constraint condition, their corresponding adjoint boundary condition and gradient expression formula are quite different. So they should be derived according to the actual situation.

2.3 Lift/drag ratio optimization in hover

For helicopter in hover, in order to minimize its required power, it needs the rotor airfoil to have a comparative higher lift/drag ratio. Therefore, its corresponding design aim is to maximize the lift/drag ratio of airfoil under the typical hovering design state, whereas to keep the lift coefficient and airfoil's sectional area almost unchanged. Typically, the objective function and design state can be written as

$$I_1 = C_D/C_L + W_1(C_L - C_L^0)^2 + W_2(A - A^0)^2$$
$$Ma = 0.6, \quad C_L = 0.6 \tag{10}$$

where C_D is the drag coefficient of the current airfoil, C_L the lift coefficient of the current airfoil, C_L^0 the lift coefficient of the baseline airfoil, A the sectional area of the current airfoil, and A^0 the area of the baseline airfoil. W_1 and W_2 are the weight coefficient.

Generally, the wall is adiabatic, so its adjoint wall boundary condition can be written as

$$\begin{cases} \Psi_2 = \dfrac{-2(\cos\alpha \cdot C_L + \sin\alpha \cdot C_D)}{C_L^2} + 4W_1 \sin\alpha (C_L - C_L^0) \\ \Psi_3 = \dfrac{-2(\sin\alpha \cdot C_L - \cos\alpha \cdot C_D)}{C_L^2} - 4W_1 \cos\alpha (C_L - C_L^0) \\ \dfrac{\partial \Psi_4}{\partial n} = 0 \end{cases} \tag{11}$$

When $\boldsymbol{\Psi}$ written as $\boldsymbol{\Psi} = (\Psi_1, \phi_1, \phi_2, \theta)$, its gradient expression can be written as

$$\delta I = 2W_2(A - A^0)\delta A - \int_B \Phi_k p_\infty \delta S_{2k} \mathrm{d}B_\xi + \int_D \frac{\partial \boldsymbol{\Psi}^T}{\partial \xi_i} \delta(\boldsymbol{S}_{ij}) f_j \mathrm{d}D_\xi - \int_D \frac{\partial \Phi_k}{\partial \xi_i} \delta \boldsymbol{S}_{ij} \sigma_{jk} \mathrm{d}D_\xi - \int_D \frac{\partial \Phi_k}{\partial \xi_i} \boldsymbol{S}_{ij} \cdot \left\{ \mu \left[\delta\left(\frac{\boldsymbol{S}_{lj}}{J}\right) \frac{\partial u_k}{\partial \xi_l} + \delta\left(\frac{\boldsymbol{S}_{lk}}{J}\right) \frac{\partial u_j}{\partial \xi_l} \right] + \lambda \delta_{kj} \delta\left(\frac{\boldsymbol{S}_{lm}}{J}\right) \frac{\partial u_m}{\partial \xi_l} \right\} \mathrm{d}D_\xi - \int_D \frac{\partial \theta}{\partial \xi_i} \delta \boldsymbol{S}_{ij} Q_j \mathrm{d}D_\xi - \int_D \frac{\partial \theta}{\partial \xi_i} \boldsymbol{S}_{ij} u_k \left\{ \mu \left[\delta\left(\frac{\boldsymbol{S}_{lj}}{J}\right) \frac{\partial u_k}{\partial \xi_l} + \delta\left(\frac{\boldsymbol{S}_{lk}}{J}\right) \frac{\partial u_j}{\partial \xi_l} \right] + \lambda \delta_{kj} \delta\left(\frac{\boldsymbol{S}_{lm}}{J}\right) \frac{\partial u_m}{\partial \xi_l} \right\} \mathrm{d}D_\xi - \int_D \frac{k}{Cv(\gamma - 1)} \frac{\partial \theta}{\partial \xi_i} \boldsymbol{S}_{ij} \delta\left(\frac{\boldsymbol{S}_{lj}}{J}\right) \frac{\partial}{\partial \xi_l}\left(\frac{p}{\rho}\right) \mathrm{d}D_\xi$$
$$i, j, k, l, m = 1, 2 \tag{12}$$

3 Grid Topology

For rotor airfoil, a structured mesh is automatically generated prior to the beginning of each iterative design step, so that the governing flow and adjoint equations can be suitably discretized. In this paper, the Thompson method is employed to solve the Poisson equations to automatically generate the C-shaped grid around the rotor airfoil. Fig. 1 shows a typical mesh around the OA209 airfoil. While employing the S-A turbulence model, normal spacing of the first grid point above the wall is set to be $0.000\,01c$ ($y^+ \approx 2$) in order to well capture the information of boundary layer. During each optimal step, it will also need to modify the grid to obtain gradient information. A simple but effective modified method[19] is adopted in this work, its form is

$$\begin{cases} x^{\text{new}} = x^{\text{old}} + N(x_{\text{airfoil}}^{\text{new}} - x_{\text{airfoil}}^{\text{old}}) \\ y^{\text{new}} = y^{\text{old}} + N(y_{\text{airfoil}}^{\text{new}} - y_{\text{airfoil}}^{\text{old}}) \end{cases} \tag{13}$$

where $N = \dfrac{\text{Length}_{\text{total}} - \text{Length}j}{\text{Length}_{\text{total}}}$.

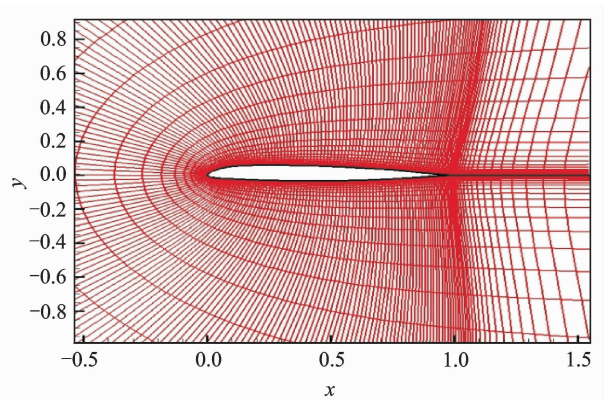

Fig. 1 Structured grid around OA209 airfoil

4 Flow Chart of Adjoint Optimal Method

Fig. 2 shows the specific flow of rotor airfoil optimization using adjoint optimal method. During each optimal process of the airfoil shape, the C-shaped body-fitted mesh is firstly automatically generated around the airfoil. Then the flowfield governing equations are solved for value of the

conservative variables, and continually their corresponding viscous adjoint equations are solved for the value of Lagrange multiplier. On these bases, the gradient information can be evaluated using the mesh deformation technique. Finally, the steepest descent method is implemented for the procedure. These works are taken repeatedly until the new airfoil satisfies the convergence criterion that the objective function value of the airfoil varies less than 1 percent of the previous step.

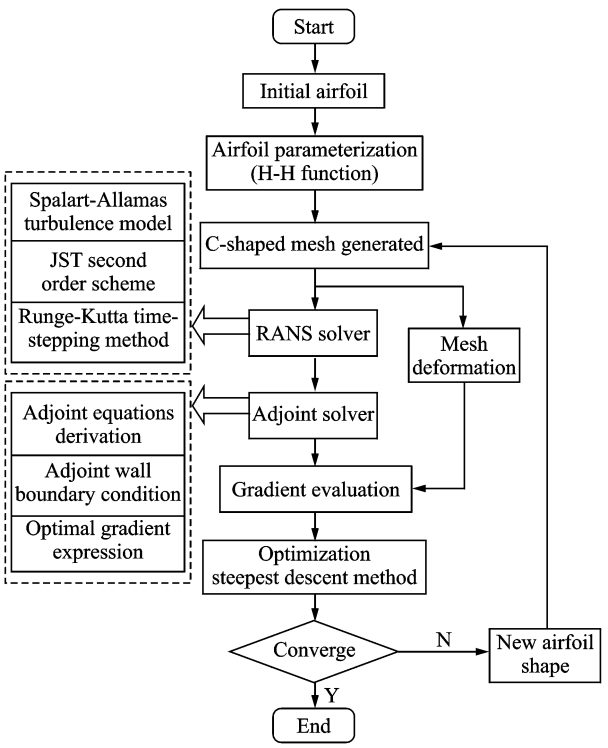

Fig. 2 Flow chart of optimization

5 Results and Discussions

5.1 Validation of flowfield of rotor airfoil

Before using the Navier-Stokes (N-S) solver for the optimal design of rotor airfoil, it needs to validate its capability to predict the flow phenomena of the typical rotor airfoil. In this section, OA209 rotor airfoil is firstly chosen to validate the rotor airfoil flow solver at state of $Ma=0.16$, AOA (Angle of attack) $=10.0°$, $Re=1.8\times10^6$. In Fig. 3, it makes a comparison of calculated pressure coefficient distributions with experimental data[6]. It is clear from the comparisons that the current flowfield solver can well simulate the flow around rotor airfoil.

Figs. 4, 5 show the lift coefficients line and the polar line of the OA209 rotor airfoil at state of $Ma=0.4$, $Re=1.4\times10^6$. To make better comparison, the experimental data[6] are also imposed on these plots. From the figures, it is shown that the current two-dimensional flow solver can well simulate the aerodynamic force of the rotor airfoil, too.

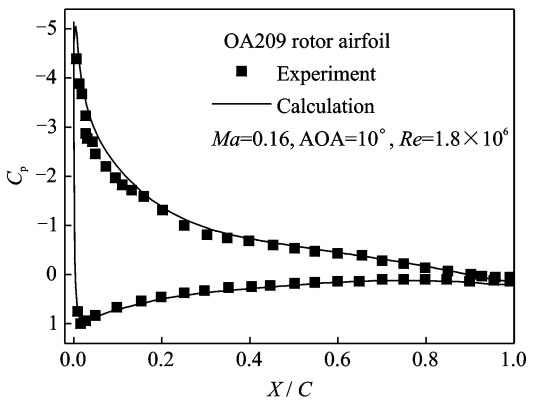

Fig. 3 Comparison of calculated pressure coefficient distributions with experimental data of OA209 airfoil

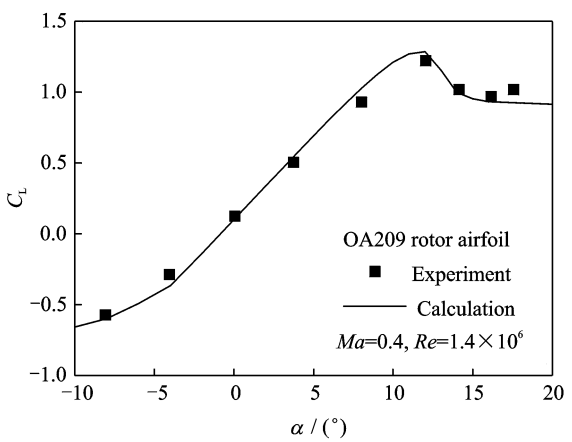

Fig. 4 Comparison of calculated lift coefficient with experimental data of OA209 airfoil

5.2 Validation of flowfield of hovering rotor

On the basis of numerical simulation of the rotor airfoil, the flowfield of the hovering rotor is also needed to testify in order to further validate the better aerodynamic characteristics of optimized new rotor. The UH-60A helicopter rotor is

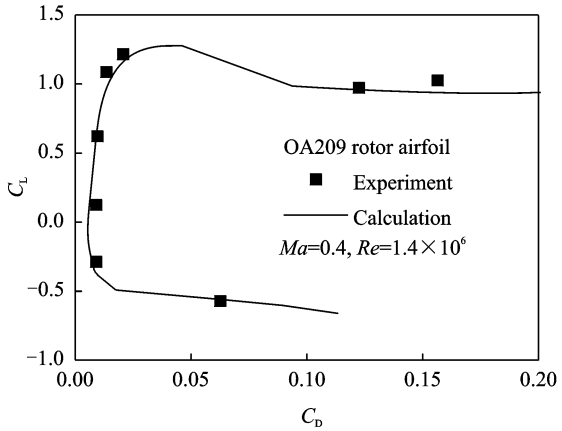

Fig. 5 Comparison of calculated polar lines with experimental data of OA209 airfoil

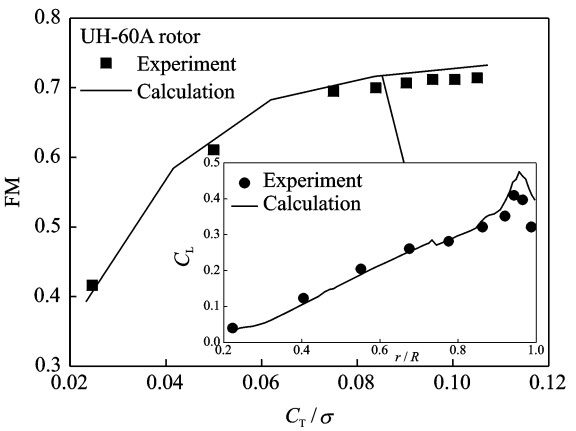

Fig. 7 Thrust coefficient and FM of UH-60A rotor

run for the simulation, which has a rearward sweep of 20° starting from 93% radius, an aspect ratio of 15.3 and a negative maximum twist of 13°.

In Fig. 6, the typical calculated pressure distributions of UH-60A rotor is compared with the experi-mental data[20] in the figure, which operates at the state of $Ma_{tip}=0.628$ and $\theta_0=9°$. From the comparison, the simulated pressure distributions on the rotor blade correlate well with the experimental data. In Fig. 7, it shows the correlation of the thrust coefficient (C_T/σ) and figure of merit (FM) of UH-60A rotor. To make better comparison, the experimental data[20] are also imposed on these plots. In addition, the blade spanwise lift coefficient distribution is also given on the lower right area. It is clearly seen from the comparisons that the present CFD solver can well simulate the aerodynamic characteristics of the hovering rotor.

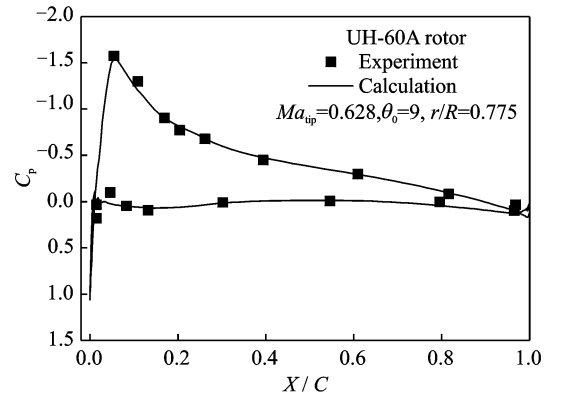

Fig. 6 Pressure coefficient distribution of UH-60A rotor

5.3 Lift/drag ratio optimization of rotor airfoil

The adjoint-based design method is now applied to design of higher lift/drag ratio rotor airfoil at hovering design state of $Ma=0.6$ and $C_L=0.6$. NACA0012 airfoil and SC1095 airfoil are chosen as the baseline rotor airfoils for optimization. For each airfoil, the surface of the airfoil is parameterized using 24 Hicks-Henne bump functions, 12 of which are distributed along the upper surface, while remaining 12 are placed in a similar fashion along the lower surface. For the objective function, the weight coefficient W_1 and W_2 are equal to 1 and 40, respectively. Because the leading edge usually has more impact on the aerodynamic characteristics, the bump functions are arranged denser in the leading edge. After around 25 steps, the optimized airfoils can be finally obtained.

For NACA0012 airfoil, Fig. 8 shows the shape and pressure distribution of baseline and optimized airfoil. After optimization, the lift/drag ratio is improved by 5.3% from 47.28 to 49.80. From Fig. 8, it is also shown that the optimized airfoil has a minor lead edge peak and adverse pressure gradient over the baseline airfoil, leading to reduce the drag coefficient to contribute a relative higher lift/drag ratio.

For SC1095 airfoil, Fig. 9 shows the shape and pressure distribution of baseline and optimized airfoil. After optimization, the lift/drag ratio is improved by 6.2% from 51.66 to 54.82. From Fig. 9, it is demonstrated that the opti-

mized airfoil has a minor peak in the leading edge but still produce a relatively higher lift in the middle region to keep lift unchanged, and it can as well reduce the drag to have a relative higher lift/drag ratio.

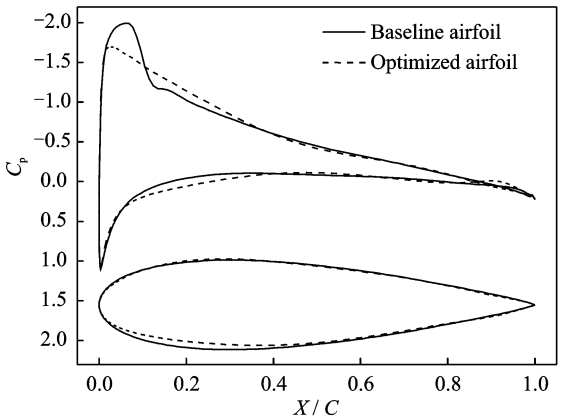

Fig. 8 Shape and pressure distribution of baseline and optimized airfoil of NACA0012 airfoil

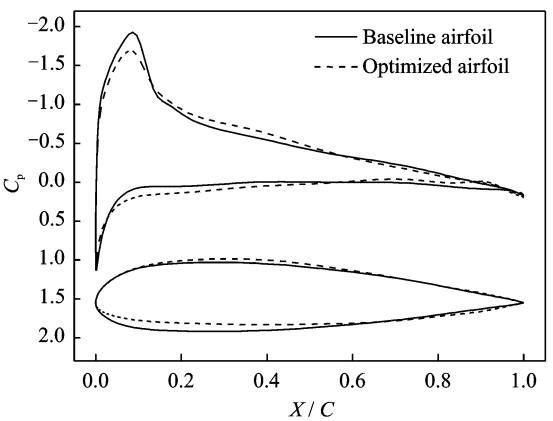

Fig. 9 Shape and pressure distribution of baseline and optimized airfoil of SC1095 airfoil

5.4 Aerodynamic performance of optimized rotor

After the optimized higher lift/drag ratio rotor airfoil is obtained, the optimized one is then continually applied to form three-dimensional rotor neglecting the influence of twist law and planform of the rotor. For the rotor, its aspect ratio is 15.0, and it operates at the state of $Ma_{tip}=0.612$ and $Re=1.92\times10^6$. In Fig. 10, it compares the hover performance of different rotors with the SC1095 baseline airfoil or optimized airfoil. From Fig. 10, we can obtain FM of the optimized one is prior to the baseline rotor, and the biggest FM of the optimized one has nearly 2.5% increase compared with the baseline rotor.

Figs. 11, 12 show the pressure coefficient distributions on the baseline and optimized rotor with different pitch angles of calculated Points 1 and 3, respectively. From the figures, it can be seen that the leading edge peak of each spanwise section of the optimized rotor is superior to the baseline rotor. In Fig. 13, it gives the streamline of the baseline and optimized rotor at calculated Point 3. From Fig. 13, it is noticed that the optimized rotor has less separation area when compared with the baseline rotor. Through the three-dimensional validations, it is demonstrated that the rotor with the optimized airfoil has better hover aerodynamic performance.

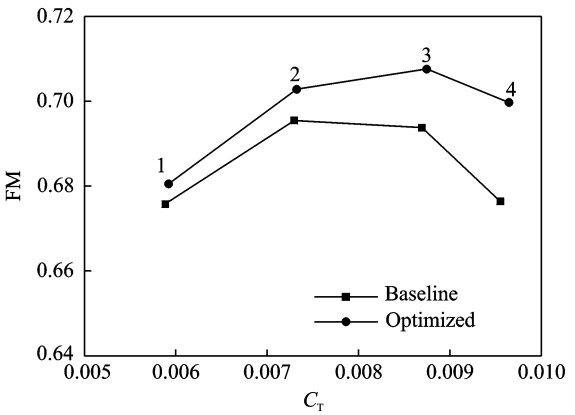

Fig. 10 Thrust coefficient and FM of baseline and optimized one of SC1095 airfoil

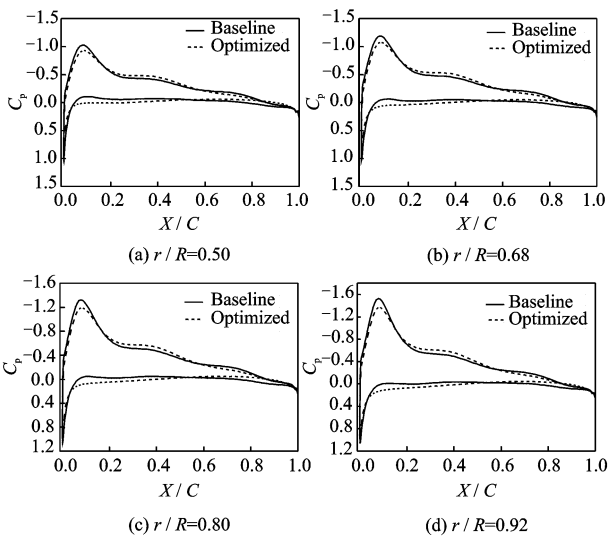

Fig. 11 Pressure coefficient distributions on baseline and optimized rotor at Point 1

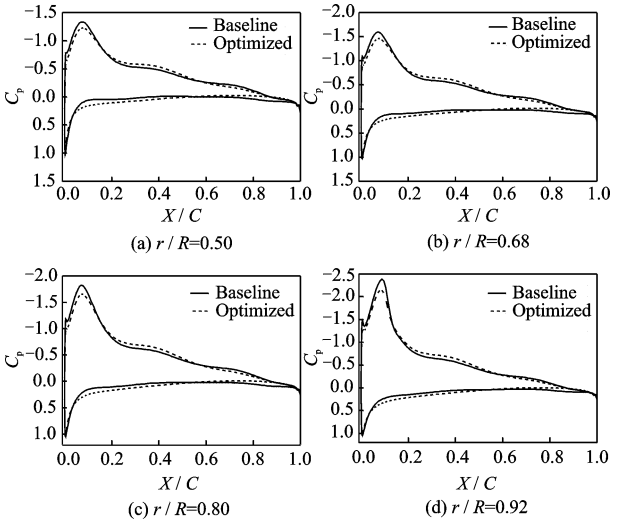

Fig. 12 Pressure coefficient distributions on baseline and optimized rotor at Point 3

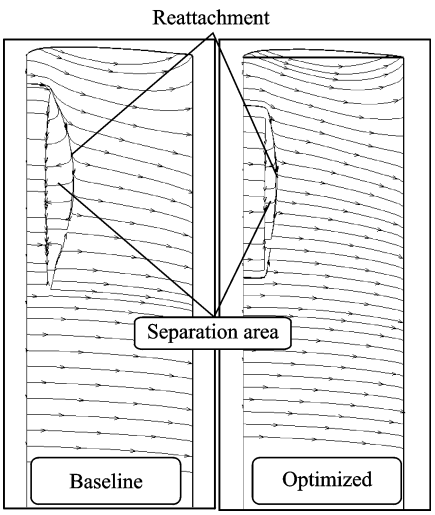

Fig. 13 Streamline of baseline and optimized rotor at Point 3

5.5 Computation costs

In present, the developed code for the viscous continuous adjoint optimal method is set up on a personal computer with Intel Core i7-4770 3.40 GHz CPU. The comparison of the computational cost of gradient information is made between the finite difference method and adjoint method for optimization of NACA 0012 airfoil's lift/drag ratio. The comparison results are given in Table 1. From Table 1, it is demonstrated that in the present design state, the computational cost is reduced by 77%. When the number of design variables becomes larger, the advantages of the adjoint method become more obviously.

Table 1 Comparisons of CPU time between the two methods

Number of design variables	Continuous adjoint method/min	Finite difference method/min
24	2.8	12.2
36	2.8	18.1
48	2.8	24.0

6 Conclusions

The highly-efficient continuous viscous adjoint method, which is suitable for the multi-constrained problem, is developed for the aerodynamic shape optimization of the rotor airfoil. Then the method is adopted to optimal design of two representative rotor airfoils with the aim of higher lift/drag ratio. Furthermore, the optimized rotor airfoil is also applied to form three-dimensional rotor to verify its hover aerodynamic characteristics compared with the baseline rotor. The following conclusions can be drawn:

(1) The continuous viscous adjoint optimal method is more efficient than the typical finite difference method for solving the gradient information, and its advantages become more obviously when the number of design variables gets larger.

(2) The adjoint-based optimal method is suitable for the lift/drag ratio optimization of the rotor airfoil in hover. After optimization, the rotor with optimized airfoil has better hover aerodynamic performance compared with the baseline rotor.

(3) The present flow solver is of high precision because it can well predict the aerodynamic characteristics of the rotor airfoil and the hover rotor.

References:

[1] DADONE L U. Design and analytical study of a rotor airfoil: NASA CR-2988[R]. 1978.

[2] LEISHMAN J G. Rotorcraft aeromechanics: Getting through the dip[J]. Journal of the American Helicopter Society, 2010, 55(1): 1-24.

[3] MALONE J B, NARRAMORE J C. Airfoil design method using the N-S equations[J]. Journal of Air-

craft, 1991,28(3):216-224.

[4] SHANG Keming, ZHAO Qijun, ZHAO Guoqing, et al. Inverse design analysis on helicopter rotor airfoils and aerodynamic shapes[J]. Journal of Nanjing Univer-sity of Aeronautics & Astronautics, 2010, 42(5):550-556. (in Chinese)

[5] VICINI A, QUAGLIARELLA D. Inverse and direct airfoil design using a multi-objective genetic Algorithm[J]. AIAA Journal, 1997,35(9):1499-1505.

[6] YANG H, SONG W P, Han Z H, et al. Multi-objective and multi-constrained optimization design for a helicopter rotor airfoil[J]. Acta Aeronautica et Astro-nautica Sinica, 2012,33(7):1218-1226.

[7] HICKS R M, HENNE P A. Wing design by numerical optimization: AIAA Paper 79-0080[R]. AIAA, 1979.

[8] BISCHOF C, CARLE A, CORLISS G, et al. Generating derivative codes from FORTRAN programs: Internal report MCS-P263-0991[R]. [S. l.]: Argonne National Laboratory and Center of Research on Parallel Computation, Rice University, 1991.

[9] MARTINS A, KROO I M, ALONSO J. An automated method for sensitivity analysis using complex variables[C]//38th Aerospace Sciences Meeting. Reno, Nevada: AIAA paper, 2000.

[10] JAMESON A. Aerodynamic design via control theory: NASA-CR-181749[R]. NASA,1988.

[11] JAMESON A, REUTHER J. Control theory based airfoil design using the Euler equations: AIAA-94-4272[R]. AIAA,1994.

[12] JAMESON A, PIERCE N A, MARTINELLI L. Optimum aerodynamic design using the Navier-Stokes equations: AIAA-97-0101[R]. AIAA,1997.

[13] KIM S, ALONSO J, JAMESON A. Design optimization of high-lift configurations using a viscous continuous adjoint method: AIAA 2002-0844[R]. AIAA,2002.

[14] JAMESON A, SRIRAM S, MARTINELLI L, et al. Aerodynamic shape optimization of complete aircraft configurations using unstructured grids: AIAA Paper 2004-533[R]. AIAA,2004.

[15] LEE S W, KHOWN O J. Aerodynamic shape optimization of rotor blades in hover using unstructured mesh[C]//60th AHS Forum. Baltimore, Maryland: [s. n.], 2004:536-547.

[16] HUANG Haisheng, YANG Xudong. Optimum shape design of rotor airfoils via control theory[J]. Aero-nautical Computing Technique, 2010, 40(4): 22-26.

[17] SPALART P, ALLMARAS S. A one-equation turbulence model for aerodynamic flows: AIAA Paper 92-0439[R]. AIAA,1992.

[18] JAMESON A, SCHMIDT W, TURKEL E, et al. Numerical solutions of the Euler equations by finite volume methods using Runge-Kutta time-stepping schemes: AIAA Paper-81-1259[R]. AIAA,1981.

[19] REUTHER J, JAMESON A, ALONSO J, et al. Constrained multipoint aerodynamic shape optimization using an adjoint formulation and parallel computers[J]. Journal of Aircraft, 1999,36(1):51-60.

[20] ABHISHEK A, DATTA A, CHOPRA I. Prediction of UH-60A structural loads using multibody analysis and swashplate dynamics[J]. Journal of Aircraft, 2009,46(2):474-490.

Mr. **Wu Qi** is a postgraduate in aircraft design at Nanjing University of Aeronautics and Astronautics, and his research interests are helicopter aerodynamics, helicopter CFD, aerodynamic shape design of high performance rotor blade.

Prof. **Zhao Qijun** is a professor and Ph. D. advisor in College of Aerospace Engineering at Nanjing University of Aeronautics and Astronautics, where he received his Ph. D. degree in aircraft design. His main research interests are helicopter CFD, helicopter aerodynamics, aerodynamic shape design of rotor blade, active flow control on aerodynamic characteristics of rotor, and rotor aero-acoustics.

Mr. **Wang Qing** is a Ph. D. candidate in aircraft design at Nanjing University of Aeronautics and Astronautics, and his main research interests are aerodynamic shape optimization of rotor airfoil and rotor blade, unsteady aerodynamics and helicopter CFD.

(Executive Editor: Xu Chengting)